Bloom succession and nitrogen dynamics during snowmelt in a mid-order montane river

H. Maurice Valett [ID] · **Rafael Feijó de Lima** [ID] ·
Marc Peipoch [ID] · **Royce C. Engstrom** [ID]

Abstract The Upper Clark Fork River (UCFR), Montana, a mid-order well-lit system with contemporary anthropogenic nitrogen (N) enrichment and natural geogenic sources of phosphorus (P), experiences annual algal blooms that influence ecosystem structure and function. This study was designed to assess the occurrence of riverine algal blooms (RABs) in the UCFR by characterizing the succession of periphyton and biogeochemical conditions following annual snowmelt runoff through autumnal baseflow conditions, and to provide a framework for assessing RAB progression in montane mid-order rivers more broadly. Using a 21-year database (2000–2020) collected over the growing season at three sites, historical assessment of the persistent and recurrent character of RABs in the UCFR showed that the magnitude of the summer bloom was, in part, moderated by snowmelt disturbance. Abundance and growth forms of benthic algae, along with river physicochemistry

(e.g., temperature) and water chemistry (N and P concentration), were measured over the course of snowmelt recession for three years (2018–2020) at the same three sites. Results documented the onset of major blooms of the filamentous green algae *Cladophora* across all sites, commensurate with declines in dissolved inorganic N. Atomic N:P ratios of river water suggest successional transitions from P- to N-limitation associated with mid-season senescence of *Cladophora* and development of a secondary bloom of N-fixing cyanobacteria, dominated by *Nostoc cf. pruniforme*. Rates of N-fixation, addressed at one of the sites during the 2020 snowmelt recession, increased upon *Cladophora* senescence to a maximal value among the highest reported for lotic systems (5.80 mg N/m^2/h) before decreasing again to background levels at the end of the growing season. Based on these data, a heuristic model for mid-order rivers responding to snowmelt disturbance suggests progression from phases of physical stress (snowmelt) to optimal growth conditions, to conditions of biotic stress later in the growing season. Optimal growth is observed as green algal blooms that form shortly after peak snowmelt, then transition to stages dominated by cyanobacteria and autochthonous N production later in the growing season. Accordingly, interactions among algal composition, reactive N abundance, and autochthonous N production, suggest successional progression from reliance on external nutrient sources to increased importance of autochthony, including

H. M. Valett (✉) · R. F. de Lima · R. C. Engstrom
Division of Biological Sciences, University of Montana, Missoula, MT 59812, USA
e-mail: maury.valett@umontana.edu

M. Peipoch
Stroud Water Research Center, Avondale 19311, PA, USA

N-fixation that sustains riverine productivity during late stages of snowmelt recession.

Introduction

Algal blooms have a conceptual origin as the episodic proliferation of planktonic algae in marine environments and can be defined as a period in time of notably enhanced autotrophic production and algal biomass accumulation (Hallegraeff 2003). Even though algal blooms are more prevalent in standing waters, their presence in lotic systems is also well documented (Bruns et al. 2022). In small to medium rivers, riverine algal blooms (RABs) typically include intensive benthic algal growth associated with nutrient-rich conditions and flow alterations (Dodds and Gudder 1992; Biggs 1996, 2000; Dodds et al. 1997). While RABs composed mostly of green algae can often be traced to either natural or anthropogenic nitrogen (N) enrichment (Biggs 2000; Heisler et al. 2008; Paerl et al. 2018), a growing body of evidence has demonstrated that lotic systems also undergo cyanobacterial blooms (Paerl et al. 2001; Power et al. 2008; Dodds and Smith 2016; Wood et al. 2020). Under appropriate conditions, cyanobacterial mats outcompete other species, not only due to their capacity to fix N, but from the production of chemicals that make them less palatable to grazers and potentially toxic to wildlife and humans (McAllister et al. 2016; Vadeboncoeur and Power 2017).

The establishment of N-fixing bacteria can also alter local biogeochemical processes to the extent that algal demand for allochthonous N may be greatly diminished, ultimately decoupling aquatic primary production from terrestrial nutrient inputs (Marcarelli and Wurtsbaugh 2009). In fact, N-fixation rates during RABs dominated by cyanobacteria have been shown to be among the highest recorded for aquatic systems (Grimm and Petrone 1997; Kunza and Hall 2014). However, mapping RABs in space and time requires knowledge of disturbance regimes, biogeochemical conditions, and non-point-source anthropogenic influences that are typically system specific (Kunza and Hall 2014; Marcarelli and Wurtsbaugh 2014).

Accordingly, the conditions that lead to blooms and enhanced cyanobacterial activity are still poorly understood. Moreover, knowledge related to RABs specifically lags behind what is known for lentic systems (Smith 1983; Moss 2012). Although similar abiotic factors (temperature, light, or nutrient availability) control algal growth in both lentic and lotic systems, these factors are more limited as predictors of RAB extent and timing. For example, correlations between nutrients and chlorophyll *a* (chl *a*) in lotic systems are generally weaker than those in non-flowing waters (Dodds et al. 2002; Bennett et al. 2017), reflecting the temporal decoupling between in situ algal growth and instantaneous abiotic conditions in the water. In lotic systems, abiotic conditions can show greater variation along flow paths than over time at a fixed location, as seems to be the case for underwater sunlight exposure (Gardner et al. 2020). In addition, well-established negative relationships between water depth and incident light in lentic systems can be hindered by high turbulence and suspended particles characteristic of particular river sections, leading to confounding patterns.

Snowmelt, succession, and RABs

Floods and droughts have been recognized as the main agents of disturbance in running waters (Poff 1992; Lake 2008). In these systems, conditions immediately following floods promote primary productivity due to increased nutrient availability and scoured substrates open to algal colonization. Whether and how successional trajectories lead to RABs and subsequent phases of cyanobacterial proliferation and N-fixation reflect a combination of biotic and abiotic factors (Fisher et al. 1982; Biggs et al. 1998; Power et al. 2008; Heffernan et al. 2010; Vadeboncoeur and Power 2017).

Successional processes and trajectories are a critical part of the temporal dynamics of montane stream systems subject to disturbance associated with snowmelt flooding (Peterson et al. 2001; Yarnell et al. 2010). In these montane systems, flood disturbance includes a sustained pulse of runoff that is highly predictable but temporally of low frequency (Poff and Ward 1989). Thus, spring snowmelt represents an annual disturbance early in the growing season that generates scour, sets initial physical and chemical

conditions, and initiates successional responses by benthic biota, including primary producers.

Following snowmelt, successional trajectories are often tightly related to biogeochemical conditions driven by both exogenous and endogenous factors. As flow declines during snowmelt recession, physical consolidation of substrates allows for algal proliferation (Marcarelli and Wurtsbaugh 2009), and retention by primary producers can deplete water column nutrients, including N, leading to senescence and sloughing (Bothwell and May 1985; Grimm 1987; Davis et al. 2012). Under P-enriched conditions, these factors can combine to promote dominance by N-fixing cyanobacteria (Grimm and Petrone 1997; Sabater et al. 2003) during later stages of succession.

Algal blooms in the Upper Clark Fork River, Montana, USA

The Upper Clark Fork River (UCFR) is a snowmelt-fed river located in western Montana, USA (Fig. 1) undergoing floodplain restoration prompted by historical metal contamination (Moore and Langer 2012). Anthropogenic N enrichment, coupled with naturally high levels of P (Ingman 1992) and well-lit channels, leads to annual RABs dominated by the filamentous alga *Cladophora glomerata* (L.) Kütz (Dodds et al. 1997; Suplee et al. 2012). Standing crops of benthic chl *a* are routinely in excess of the 100 mg/m^2 threshold set as a water quality standard for the river (Suplee et al. 2009), and are often above 600 mg/m^2 (Suplee et al. 2012).

Results from the UCFR Long-Term Research in Environmental Biology (LTREB) program (D'Andrilli et al. 2021), a monitoring network that has been in place since 2017, demonstrate that the N inputs occur mainly over the first 40 km of the river (Kyro 2021) and that downstream reaches are rich in P due to geogenic sources (Valett et al. 2022). During warm summer baseflow, conditions favor secondary blooms of N-fixing cyanobacteria (mostly *Nostoc cf. pruniforme*). Little is known about the successional trajectory of RABs in the UCFR and the potential influences of a secondary cyanobacterial bloom. Information on these secondary blooms is of interest given efforts to reduce N loads in the UCFR (Suplee et al. 2012) and current concerns over enrichment in the context of ongoing restoration efforts.

In this study, we combine historic and contemporary work on the UCFR to address the successional character of RABs and their potential to alter the river's biogeochemistry. We combine data sets from long-term monitoring of the growing season over 21 years (2000–2020) at three sites, temporally intensive UCFR LTREB data covering the progression of snowmelt recession for three years (2018–2020) from the same sites, and a focused study of algal succession and N-fixation at a single site for one year (2020) to address five objectives: (1) characterize historic spatial and temporal patterns in physicochemical conditions, (2) address historic RAB intensity and its relationship to spring flooding, (3) document the temporal progression of the biogeochemical template during snowmelt recession, (4) use periphyton growth forms and pigment content to characterize successional change in summer algal blooms with emphasis on the shift from filamentous green algae to epilithic cyanobacteria, and (5) provide a functional assessment of the seral progression (i.e., successional character) of N-fixation, and tie rates to environmental conditions driving autochthonous N inputs and cyanobacterial abundance.

Methods

Historical datasets

Historical datasets for physicochemical conditions, nutrient (N and P) concentrations, and summer algal biomass (as organic matter and chl *a*) for the three focal study sites were obtained from the Water Quality Data Portal (National Water Quality Monitoring Council, https://acwi.gov/monitoring/). Data were obtained for 3 locations (Fig. 1; Site 1, Deer Lodge; Site 2, Garrison; and Site 3, Bonita – designated from upstream to downstream) along the UCFR. These sites are a subset of monitoring stations that have been historically sampled by the Tristate Water Quality Council (2009) and the Montana Department of Environmental Quality (MT-DEQ) during the growing season over four decades (site codes: TSWQC_WQX-CFROP-9, TSWQC_WQX-CFROP-10 and TSWQC_WQX-CFROP-12). Long-term measures of summer algal abundance include total organic matter and total chl *a* without distinction among algal growth forms. Historical
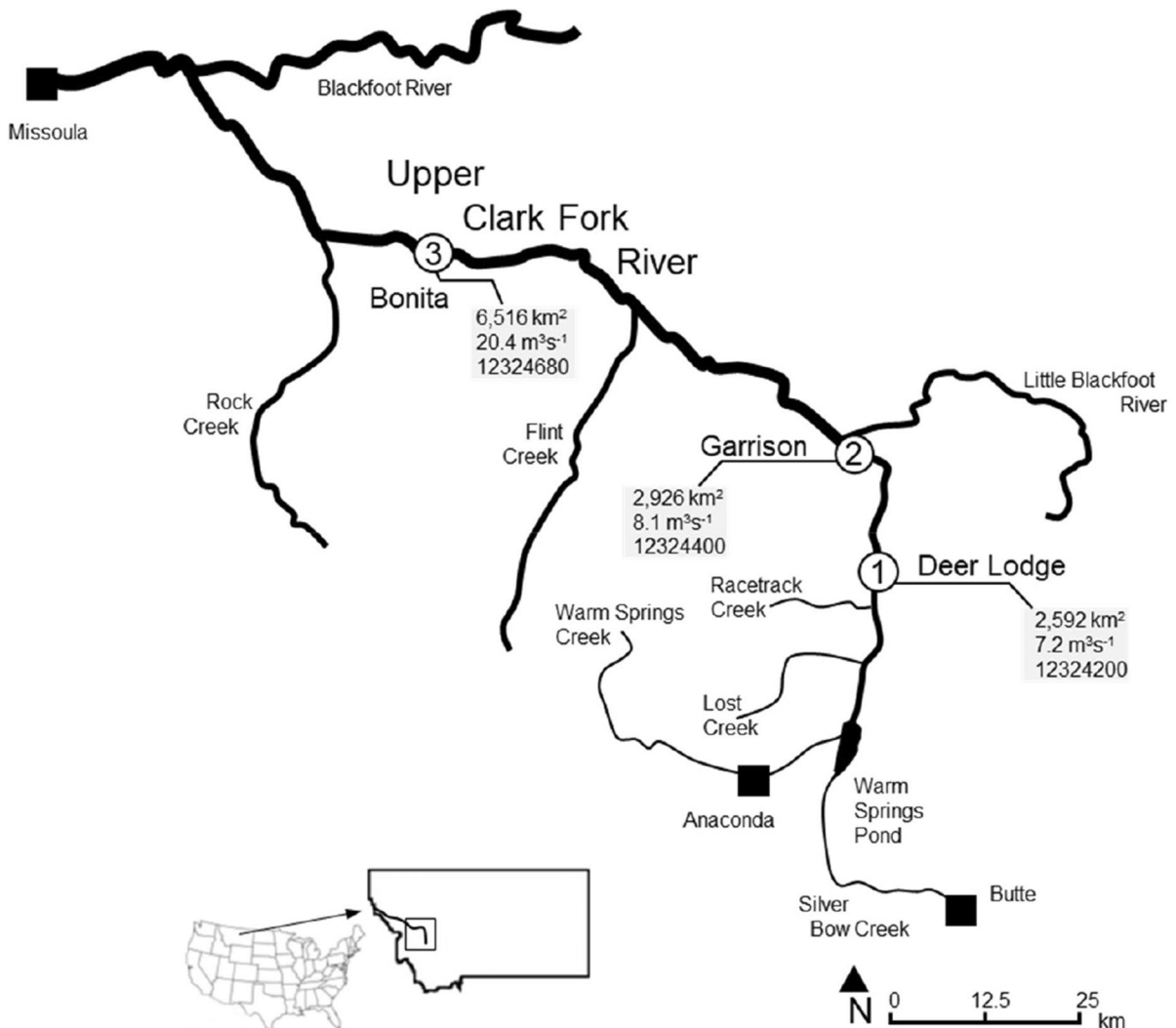
Fig. 1 Map of the study area on the Upper Clark Fork River (UCFR) and significant tributaries showing the three long-term monitoring locations (circled numerals, 1–3). UCFR catchment area, average annual discharge (1984–2013), and USGS gauge numbers associated with each of the monitoring loca-

tions are provided in the grey boxes. Historical mining operations in Butte and Anaconda (black squares) located on Warm Springs and Silver Bow Creeks led to the construction of Warm Springs Pond at the origin of the UCFR for the purpose of retaining metal- contaminated sediments

data from these sites (2000–2020) include multiple measures within a year that were used to generate annual means for growing season conditions (July–September). Long-term sites were chosen for the extent and completeness of datasets, but also because they coincide with areas currently studied by our program. A thorough description of the methods of collection and analysis of these nutrient and algal biomass datasets can be found in Suplee et al. (2012).

2018–2020 monitoring datasets

Along with a number of other sites, the UCFR LTREB program monitors water quality at these three sites year-round. Samples are taken every two weeks during the growing season and monthly during the rest of the year. During the 2018 to 2020 period, nutrient concentrations were determined from triplicates samples collected at each site using HDPE bottles, filtered in the field (Whatman GF/F, 0.7-µm pore

size) into polypropylene tubes, stored on ice for transport, and frozen in the laboratory until analysis. Filtered water samples were analyzed for soluble reactive phosphorus (SRP, mg/L), nitrate–N (NO_3-N), and ammonium-N (NH_4-N) using a segmented flow analyzer (Astoria-Pacific AP2, Clackamas, OR). Analysis of NO_3-N was performed using cadmium-reduction chemistry (EPA 1993a), NH_4-N according to the phenol-hypochlorite colorimetry method (EPA 1993b), and SRP concentrations determined using the ascorbic acid colorimetry method (EPA 1993c). Dissolved inorganic nitrogen (DIN) was calculated as the sum of NO_3-N and NH_4-N. Temperature (°C), specific electrical conductivity (µS/cm), and dissolved oxygen (mg/L, % saturation) were measured using a YSI sonde (YSI, ProSolo, Yellow Springs Instruments, Irvine, CA).

During 2020, comprehensive sampling of RAB progression was initiated at the three focal sites as soon as possible after peak flow (July 13th), and continued weekly until mid-October. At each site, we collected 5 samples of benthic algae using a cylindrical benthic sampler (30-cm diameter, area = 0.08 m^2). When present, filamentous algae were removed from the surface of all rocks contained within the sampler. The remaining growth forms (stalked, short filaments, and adnate) in the periphyton (e.g., epilithon) were removed from the rocks using a wire brush. Filamentous and epilithon samples were kept separate, taken to the laboratory on ice, and processed within 24 h of collection. For each growth form, benthic organic matter (BOM) standing stocks were measured as ash-free dry mass (AFDM, g/m^2). Collected materials were analyzed for AFDM following standard protocols; dry mass was measured following 24 h at 60 °C, and ash mass after sample ignition for one hour at 550 °C, cooling and re-weighing. For slurries of epilithon, subsamples were filtered through pre-weighed Whatman GF/F (0.7-µm pore size) filters. For filamentous algae, subsamples of wet weight were used for drying and combustion.

Samples were analyzed for chl a and phaeophytin using 90% buffered acetone for pigment extraction and spectrophotometric assessment with acidification following Steinman et al. (2017). Phycocyanin standing crops extracted in water from epilithic samples were obtained through the use of a handheld fluorimeter (Aquafluor 8000, Turner Designs, Sunnyvale, CA, USA) following Moulton et al. (2009) and

Cremella et al. (2018). Final standing crops for biomass and pigments were calculated including corrections for sub-sampling volumes and were normalized to sampling area.

2020 N-fixation study

Nitrogen fixation assays were performed across 15 dates between July 13th and October 7th 2020 at the downstream-most site (Site 3—Bonita). We chose Site 3 for our study because it is a location observed to have early spring *Cladophora* blooms and evident late season blooms of N-fixing cyanobacteria. For each sampling date, nutrient concentrations in the water column were determined following methods previously indicated. Acetylene reduction assays (Capone 2018; Eberhard et al. 2018), executed on each sampling date included filling 6 2-L plastic chambers with rocks randomly selected from the study reach and incubating them in water saturated in acetylene. Acetylene was generated in the field using the reaction between calcium carbide and water and acetylene gas was injected through a septum in the chamber using a syringe, creating a 200-ml headspace. Chambers were placed in the river so as to standardize for water temperature and depth along an 8- to 12-m reach where water flow was present but not strong enough to move or disturb the chambers. A sample of 5 ml from the headspace was retrieved after 2 h of incubation and placed in evacuated tubes for analysis in the lab. For all dates, an extra chamber containing only river water was also incubated as a field-blank and ethylene production was never detected in those samples. Ethylene content was determined using an SRI Greenhouse gas analyzer equipped with a flame ionization detector and Poropak R columns (oven temperature 80 °C) with N_2 carrier gas flow (80 mL/min).

A temperature logger (HOBO Model UA-002-64, Onset Computer Corporation, Pocasset, MA) was placed inside each chamber to determine average water temperature during incubation. A LiCor Underwater Photosynthetically Active Radiation (PAR) sensor coupled with a logger (LI-192, LI-1401, LI-COR Inc., Lincoln, Nebraska, USA) was placed in the middle of the incubation reach and PAR was normalized for all individual chambers accounting for beginning and end of incubation times. Across all dates, incubation times ranged from 9am to 3 pm. At the end

of incubation, epilithic and filamentous algae were removed from the rocks and processed separately for pigments (chl *a*, phaeophytin, and phycocyanin) and biomass standing stocks using the same methods used to monitor the three study sites, but with stocks normalized to surface area of incubated rocks.

Statistical methods

All values presented in the results section represent means ± standard errors unless otherwise stated. Statistical tests were carried out using the Statistical Analysis System (SAS, Cary, NC, ver 9.1) or R (R Core Team 2022). Data sets were assessed using Kolmogorov–Smirnov tests and, when appropriate, ln-transformed to meet assumptions of normality.

Objective 1: historical spatial and temporal patterns in UCFR physicochemistry: 2000–2020

Patterns in chemical conditions and bloom character were addressed using the 2000–2020 historical data sets. With location as the single factor, a one-way analysis of variance (ANOVA) followed by Student–Newman–Keuls (SNK) multiple comparison tests was used to compare mean values for physicochemical measures and nutrient concentrations among the three study sites.

Objective 2—historical algal blooms, RAB magnitude, and flood intensities: 2000–2020

Pearson correlation coefficients were calculated to address the relationship between BOM and chl *a* across sites over the 21-year historical record (2000–2020) using ln-transformed data to achieve normality across orders of magnitude. The relationships between periphyton standing crop and the magnitude of annual flooding (i.e., maximum discharge) were addressed using linear regression of ln-transformed annual mean values for chl *a* and BOM vs. maximum discharge (Q_{max}) over the same time period. To address potential for the magnitude of flooding during previous years to influence bloom development during any given growing season, maximum flows were lagged by 1, 2, and 3 years and similar regressions executed using ln-transformed means for either chl *a* or BOM standing crops.

Objective 3—snowmelt recession and temporal progression of the riverine biogeochemical template: 2018-2020

For seasonal progression of physicochemical and biogeochemical conditions during 2018–2020, measures of nutrient concentrations were normalized to local annual mean values to account for spatial variation among sites (see Valett et al. 2008). For each site and year, mean values for given sampling dates (n = 3 per date) were used as individual observations and converted to Z-scores using Eq. (1):

$$Z_i = \frac{(y_i - \bar{y})}{S}. \tag{1}$$

where: y_i is the individual observation, y-bar is the annual mean value, and S is the standard deviation for individual observations during a given sampling year. Mean Z-scores across the three years were then plotted to provide a summary description of temporal patterns of change for the three years and sites combined.

Objective 4—bloom progression and succession of algal growth forms: 2020

Linear regressions were used to address RAB succession at Site 3 during the 2020 snowmelt recession sequence. Mean standing crops of algae (as chl *a* in filamentous form) and cyanobacteria (phycocyanin abundance in epilithic samples) were regressed against time to address temporal progression of algal growth forms over a 91-day sequence.

Objective 5—seral assessment of N-fixation rates, physicochemical conditions, and biotic drivers: 2020

River substrates placed in chambers were used to assess rates of N-fixation at Site 3 during the 2020 snowmelt recession. Individual chambers (n = 6 per date) thus provided independent measures of periphyton growth forms, N-fixation rates, water temperature, and PAR on each sampling date. Replicate water samples (n = 3) were taken from the river and used to characterize water chemistry during the

monitoring period. Samples were not taken on the final date (October 7, 2020) of fixation assessment.

Linear regressions of epiphytic BOM and phycocyanin standing crops versus time were run to address temporal progression of algal growth forms on incubated riverine substrates using mean values for standing crops across the temporal sequence. Bivariate linear regressions of temperature, PAR, and phycocyanin versus ln-transformed N-fixation rates used independent chamber values to address the influences of these individual and chamber-specific environmental factors on autochthonous N production. We performed stepwise multiple linear regression in order to identify which combination of environmental variables were the best predictors of N-fixation. We compared models using temperature, light (i.e., PAR) and phycocyanin content of algal mats as predictors of N-fixation rates. Prior to fitting the multiple linear regression models, potential collinearity of predictors was assessed by calculating variance inflation factors (VIF). Collinearity between predictors was considered high when VIF > 5 (Menard 2001). Normality of residuals was tested using a Shapiro–Wilk test; residuals were inspected, and variables were transformed to achieve homoscedasticity when appropriate. Model selection was based on the lowest Akaike's information criteria (AIC, Burnham and Anderson 2002) using the *MuMIn* package in R (Bartoń 2017). Finally, we used linear regression of

mean concentrations for DIN versus mean N-fixation rate, and non-linear regression of mean SRP concentration versus mean N-fixation rate, to address how river chemistry may be related to N-fixation across the 13 observations.

Results

Historical spatial and temporal patterns in UCFR physicochemistry: 2000–2020

Over the 20-year monitoring period, average growing season temperatures ranged only 0.9 °C (16.3 to 17.1 °C, Table 1) across sites while daytime DO (8.7 – 9.5 mg/L) and % saturation (> 90%) remained high (Table 1). Concentrations of NO_3-N declined directionally among sites from 0.096 mg/L at Site 1 to 0.028 mg/L and 0.006 mg/L at Sites 2 and 3, respectively. At Sites 1–3, NH_4-N concentrations were similar and consistent (0.015, 0.015 and 0.014 mg/L, respectively, Table 1), but constituted progressively more of the DIN pool as NO_3-N declined (71% at Site 3). SRP was abundant across sites; concentrations increased downstream from 0.011 mg/L at Site 1 to nearly double that at Site 3 (0.020 mg/L, Table 1). Lower DIN and greater SRP concentrations resulted in atomic N:P declining from 49.4 at Site 1 to 9.4 and 4.3 at downstream

Table 1 Physicochemical conditions and nutrient concentrations for three monitoring sites on the Upper Clark Fork River, MT. Values are grand means[¥], lower 95% confidence limit, upper 95% confidence limit, and n based on sampling during the growing season (July–September) from 2000–2020

Parameter	Site 1 (Deer Lodge)	Site 2 (Garrison)	Site 3 (Bonita)
Temperature (°C)	16.3[A] 15.7, 16.8 (127)	16.4[A] 15.9, 17.0 (127)	17.1[A] 16.6, 17.6 (127)
Dissolved oxygen (mg/L)	9.4[A] 9.2, 9.6 (121)	9.5[A] 9.2, 9.7 (122)	8.7[B] 8.5, 8.9 (120)
Dissolved oxygen (%)	98.0[A] 93.6, 102.4 (61)	96.0[A] 91.0, 101.0 (62)	92.7[A] 88.6, 96.8 (61)
Specific conductivity (µS/cm)	426.8[B] 413.3, 440.4 (127)	437.4[B] 426.0, 448.8 (127)	462.0[A] 449.4, 474.5 (127)
pH	8.39[A] 8.34, 8.43 (126)	8.38[A] 8.33, 8.43 (126)	8.31[A] 8.27, 8.36 (126)
NH_4-N (mg/L)	0.015[A] 0.013, 0.018 (107)	0.015[A] 0.013, 0.016 (116)	0.014[A] 0.012, 0.016 (99)
NO_3-N (mg/L)	0.096[A] 0.084, 0.108 (149)	0.028[B] 0.020, 0.036 (112)	0.006[C] 0.005, 0.008 (120)
SRP (mg/L)	0.011[B] 0.010, 0.013 (139)	0.018[A] 0.016, 0.020 (157)	0.020[A] 0.016, 0.023 (135)
Atomic N:P[*]	49.4[A] 37.4, 61.3 (140)	9.4[B] 6.0, 12.8 (73)	4.3[B] 3.0, 5.6 (75)
TN (mg/L)	0.323[A] 0.307, 0.339 (145)	0.310[A] 0.292, 0.327 (167)	0.259[B] 0.244, 0.274 (140)
TP (mg/L)	0.029[B] 0.025, 0.032 (147)	0.041[A] 0.036, 0.045 (168)	0.023[B] 0.019, 0.027 (145)

[¥]Mean values within a row with unique superscripts are significantly different ($p < 0.0001$) following ANOVA and Student Newman Keuls multiple comparison test

[*]Atomic N:P derived from molar concentrations of NH_4-N, NO_3-N and SRP

sites. Concentrations of TN declined directionally among sites, but were 3-times higher than DIN concentrations at Site 1, 7-times higher at the Site 2, and 10-times higher than DIN at the Site 3 (Table 1). In contrast, TP concentrations were twice as high as mean SRP concentrations at Sites 1 and 2, but similar to SRP at the most downstream site (Table 1).

Historical algal blooms, RAB magnitude, and flood intensities: 2000–2020

From 2000–2020, mean growing season algal standing crops (i.e., chl *a*) varied more than sixfold within each of the three sites, while BOM stocks were even more variable (8- to 13-fold, Fig. S1 in Supplemental Information). Maximum mean chl *a* was measured at Site 2 in 2005 (378.4 ± 83.9, mean $\pm 95\%$ C.I.) while greatest mean BOM was observed at Site 1 in 2002 (186.1 ± 57.5) Across years and sites, 74% of annual mean chl *a* measures exceeded the 100 mg/m^2 nuisance threshold (dotted line; Fig. S1 in Supplemental Information, a, c, e). Neither chl *a* nor BOM showed a clear trend for increase or decline at any site over 20 years of monitoring. There was very strong evidence that BOM and chl *a* standing crops were positively correlated across all sites and years (Pearson correlation of BOM and chl *a*: $R = 0.78$, $p < 0.0001$, n = 2940; Fig. S2 in Supplemental Information), linking organic matter accumulation to in-stream autotrophy.

Strong evidence suggested that average growing season algal biomass was inversely related to the maximum discharge recorded during snowmelt (regression ln-transformed average growing season standing crops versus maximum discharge: $R^2 = 0.24$, $p < 0.001$, n = 63 for BOM or chl *a* vs. Q_{max}; Fig. 2), while there was little to no evidence that maximum discharge from up to three years prior affected algal abundance during any given growing season (comparable regressions using temporally-lagged maximum discharge; $p = 0.16$ to 0.24, n = 63). Assessment of the relationship within individual sites (data now shown) revealed that flood magnitude and chlorophyll standing crops were closely related at Sites 1 ($R^2 = 0.37$, $p = 0.003$) and 3 ($R^2 = 0.38$, $p = 0.002$), but were unrelated at Site 2 ($R^2 = 0.05$, $p = 0.35$).
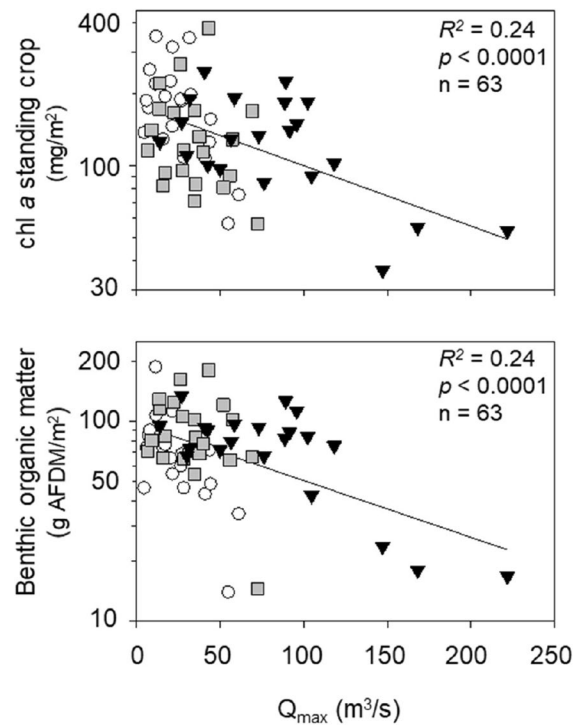

Fig. 2 Annual average standing crop for chlorophyll a (chl *a*, mg/m^2) and benthic organic matter (g AFDM/m^2) versus annual maximum discharge (Q_{max}, m^3/s). Data are mean values for each of 21 years of monitoring (2000–2020) derived from 22–79 measures annually at Site 1 (open circles), Site 2 (filled squares), and Site 3 (filled triangles)

Snowmelt recession and temporal progression of the riverine biogeochemical template: 2018–2020

During 2018–2020, peak discharge in the UCFR occurred in early spring (May 2019, June 2018 and 2020) associated with snowmelt, minimum discharge was observed in August or early September, and flow gradually increased with autumnal progression (Fig. S3 in Supplemental Information). Flow was generally similar at Sites 1 and 2; discharge increased at Site 2 by only 6.6% across monthly hydrographs for the three monitoring years. Peak flows at these two sites ranged from 22.4 to 48.4 m^3/s with maximal discharges 10–25% greater at Site 2 than at Site 1. Flow was 2 to threefold greater at Site 3 compared to upstream sites (Fig. S3 in Supplemental Information) reflecting location along the continuum via the influence of intervening tributaries (Fig. 1).
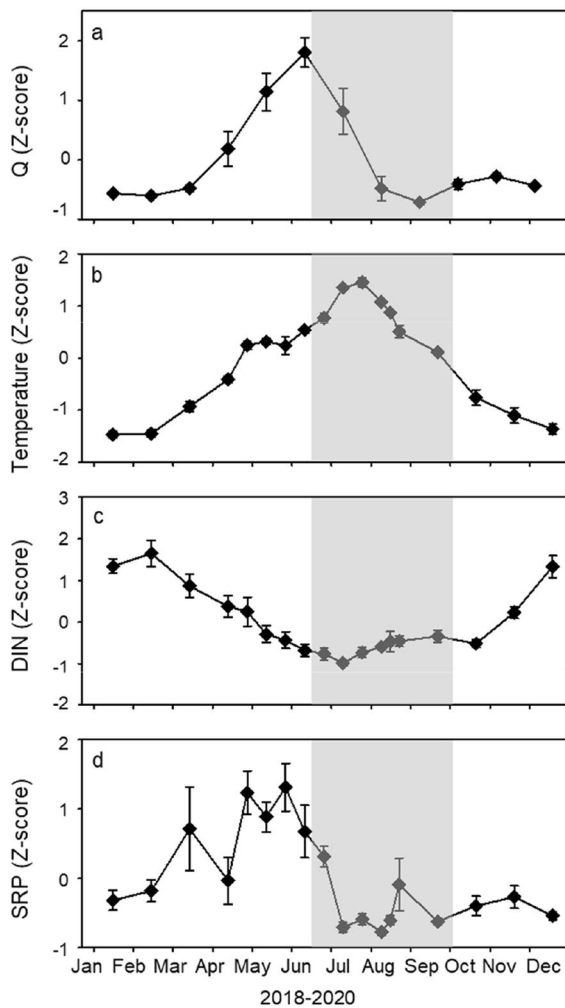
Fig. 3 Mean Z-score calculations across sites derived from three years of river monitoring (2018–2020). **a** Z-scores for river flow (Q) based on mean monthly discharge from USGS gauges at each site. Z-scores for **b** water temperature, **c** dissolved inorganic nitrogen (DIN), and **d** soluble reactive phosphorus (SRP) calculated using mean values from 17 sampling events executed annually from 2018–2020. Shaded area denotes the snowmelt recession successional period

Fig. 4 Temporal progression of N:P ratios for the UCFR (mean ± SE) across all sites as, **a** atomic abundance, and **b** Z-score calculations across all sites derived from three years of river monitoring (2018–2020). Atomic N:P ratios were calculated using mean values from replicate (n = 3) samples taken during 17 sampling events executed annually from 2018–2020. Shaded area denotes the snowmelt recession successional period. The dashed line in **a** is the Redfield Ratio of 16

While concentrations of N and P differed among sites (Table 1), Z-scores for physicochemical constituents reveal a recurrent pattern of change in the biogeochemical template at each location associated with flooding and snowmelt recession (Fig. 3). Greatest flows occurred in association with ascending temperatures which maximized in Augu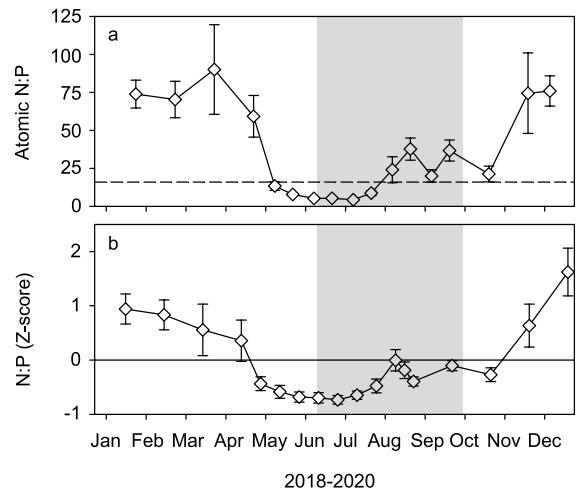st as discharge approached baseflow during the middle stages of the growing season (Fig. 3a, b). Increasing discharge coincided with declining DIN and lowest concentrations occurred in July during times of lower discharge (Fig. 3a, c). In contrast, SRP concentrations were greatest across all sites at times of higher flow, then declined dramatically during snowmelt recession to similarly minimal concentrations across all sites (Fig. 3d). As a result of changes in N and P abundance (Fig. 3c, d), atomic N:P ratios progressed predictably across seasons (Fig. 4) with mean values near 75 during winter, declining abruptly with onset of snowmelt, and remaining below the Redfield ratio (16) for most of the growing period (Fig. 4a). Spatial variation in temporal progression among sites was evident, especially for the winter periods, reflecting upstream to downstream differences in nutrient abundance. Calculated Z-score values, however, indicate robustly low N:P ratios during the growing season at all sites (Fig. 4b). Thus, the recession period was characterized by declining flow, warming, and then cooling of the water column, and decreases in bioavailable forms of N and P with concomitantly low atomic N:P ratios.

Fig. 5 Benthic chlorophyll *a* (chl *a*, mg/m^2) and phycocyanin (µg/m^2) standing crops at Site 1 (**a**, **b**), Site 2 (**c**, **d**) and Site 3 (**e**, **f**) during the 2020 growing season (July–October). Bars are mean values (+ standard error) with total height in **a**, **c**, and **d** reflecting summed abundance of filamentous and epilithic forms
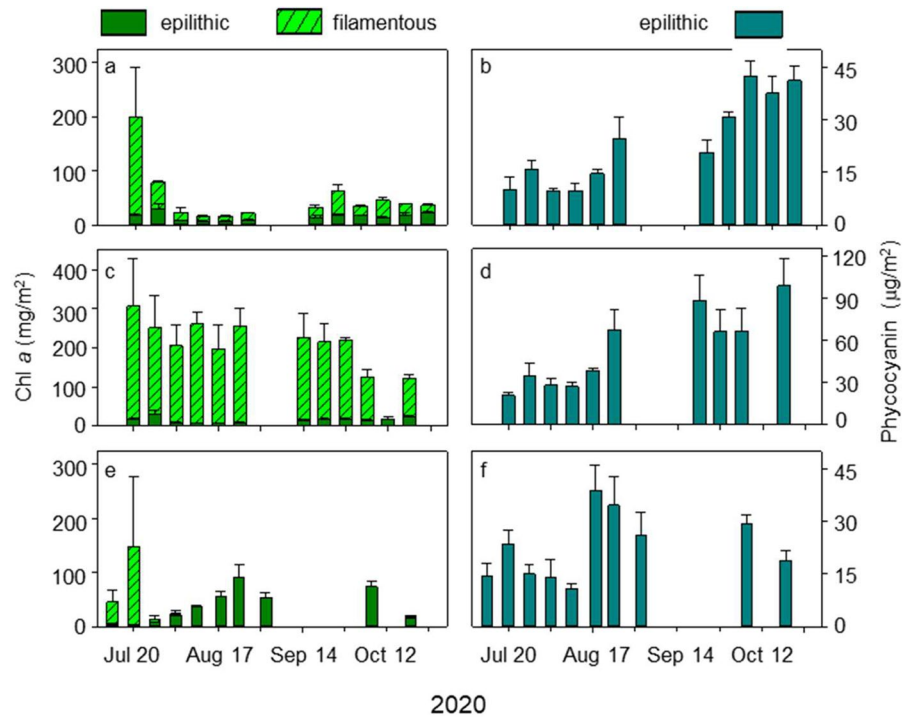
Bloom progression and succession of algal growth forms: 2020

Filamentous green algae, mostly *C. glomerata*, dominated early phases of snowmelt recession at all sites with chl *a* standing crop ranging from 145 to 219 mg/m^2 during the first few weeks of sampling (Fig. 5a, c, e). After the first two weeks, conspicuous blooms of filamentous algae collapsed at Site 1, although small tufts were present throughout the sampling period.

Filamentous forms at Site 3 also collapsed after two weeks and were effectively absent thereafter (Fig. 5a, c). At Site 2, filamentous forms persisted during almost the entirety of the growing season, but declined linearly with time (linear regression of filamentous chl *a* vs. time, $R^2 = 0.78$, $p = 0.003$, n = 12); maximal chl *a* standing crop occurred on the first day of monitoring at 219.0 ± 122.3 mg/m^2 and averaged 150.5 ± 18.1 mg/m^2 across all dates. Senescence of the filamentous bloom at Site 2 was observed only during the last 2–3 sampling dates (Fig. 5b). Throughout the 2020 growing season, adnate epilithic algae persisted as a component of the periphyton with chl *a* standing crops averaging 14.9 ± 2.0, 66.2 ± 5.7, and 36.2 ± 9.9 mg/m^2 at Sites 1–3, respectively (Fig. 5a, c, e).

All sites exhibited a transition to increased abundance of cyanobacteria, generally following the decline in the abundance of filamentous forms (Fig. 5b, d, f). Cyanobacterial standing crops increased linearly (regression of phycocyanin vs. time: Site 1, $R^2 = 0.84$, $p < 0.0001$, n = 11; Site 2, $R^2 = 0.81$, $p = 0.0003$, n = 10) and roughly fourfold from 9.9 to 41.0 and 20.8 to 99.0 µg/m^2 (Fig. 5b, d) at Sites 1 and 2, respectively. While the increase in phycocyanin was more gradual and similar at Sites 1 and 2, pigment standing crop at Site 3 increased abruptly after 36 days, then declined thereafter with little evidence that change was directional with time (regression of phycocyanin vs. time, $R^2 = 0.10$, $p = 0.37$, n = 10).

Seral assessment of N-fixation rates—physicochemical and biotic drivers: 2020

Physicochemical conditions

Physical, chemical, and biological features interacted to influence ecosystem succession as illustrated by the time course of algal development and N-fixation at Site 3. Photosynthetically active radiation (PAR) decreased over the temporal span of sampling; photon

flux density was greatest (1811.3 ± 3.0 µmol quanta/ m^2/s, mean $\pm$ SE across all chambers) on July 27th and least (676.7 ± 23.3 µmol quanta/m^2/s) during overcast conditions on the second to last assay date (September 23rd, Table S1 in Supplemental Information). Accordingly, chamber incubation temperatures were greater during the first half of the experiment (20.5 ± 0.17 °C, mean $\pm$ SE across all chambers for the first 7 sampling dates), followed by a marked decline and stabilization around an average of 13 ± 0.1 °C during September (Table S1 in Supplemental Information).

River concentrations of N and P reflected the downstream dominance by NH_4-N, and relatively high concentrations of SRP (Table 1; Fig. 6a, b). For all sampling dates, DIN was composed mostly of NH_4-N, with generally stable and low NO_3-N concentrations (0.001 to 0.004 mg/L) representing only 22% of DIN (Fig. 6a). Comparably low NH_4-N

concentrations were observed on the first day of monitoring (0.002 mg/L), but later increased and reached a maximum of 0.022 mg/L on July 30th, prior to decreasing to values around 0.009 ± 0.001 mg/L after August 13th. SRP concentrations generally followed a pattern opposite of that observed for NH_4-N, with maximal concentrations (0.006–0.010 mg/L) during the early and late stages of the progression, and minimum values approaching detection level (0.001 ± 0.0005 mg/L), roughly coinciding with times of peak NH_4-N concentration (Fig. 6b). Concentrations of SRP then increased to 0.005 and 0.006 mg/L during the final assay dates.

Reflecting shifts in concentrations of inorganic N and P, atomic N:P ratios changed temporally, crossing the Redfield ratio of 16. (Fig. 6c). During July, N:P ratios were lowest (0.7 to 5.9), but increased with time to a maximum on August 10th at a value of 24.3 ± 4.8, declining progressively thereafter to values less than 5 by the end of September (Fig. 6b). For 12 out of 14 sampling dates, atomic N:P ratios suggested potential N-limitation to primary productivity (i.e., N:P < 16); on two sampling dates (August 3 and 10) ratios suggested potential limitation by P abundance when ambient concentrations of SRP were 0.003 and 0.002 mg/L, respectively.
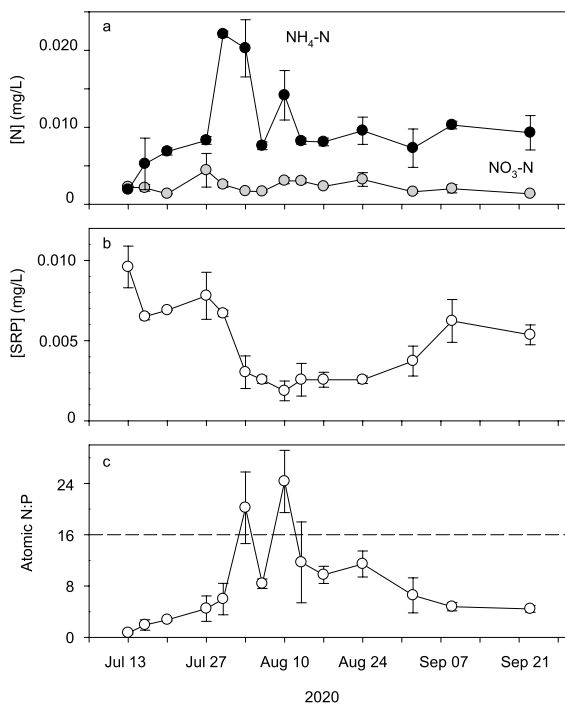
Periphyton development

As expected, the time course of algal development on rocks incubated for N-fixation assays at Site 3 followed that of the larger riverine system (Figs. 5, 7). During the first three sampling dates, periphyton was dominated by macroscopic accumulations of *C. glomerata*. Standing crops accumulated rapidly reaching an individual value as high as 989 g/m^2 AFDM and an average value of 369.0 ± 77.6 g/m^2 by the second sampling date (Fig. 7a). Abundance of filamentous algae declined rapidly thereafter (Fig. 7a); *Cladophora* mats showed signs of senescence with filaments turning a yellowish color followed by the appearance of small drifting tufts of filamentous green algae. In the following days, *Cladophora* was entirely absent in the periphyton.

Over the course of the growing season, the periphyton community became increasingly dominated by epilithic algae, more adnate in character. Following the abrupt decline in filamentous forms, epilithic biomass increased linearly (regression of epilithic BOM
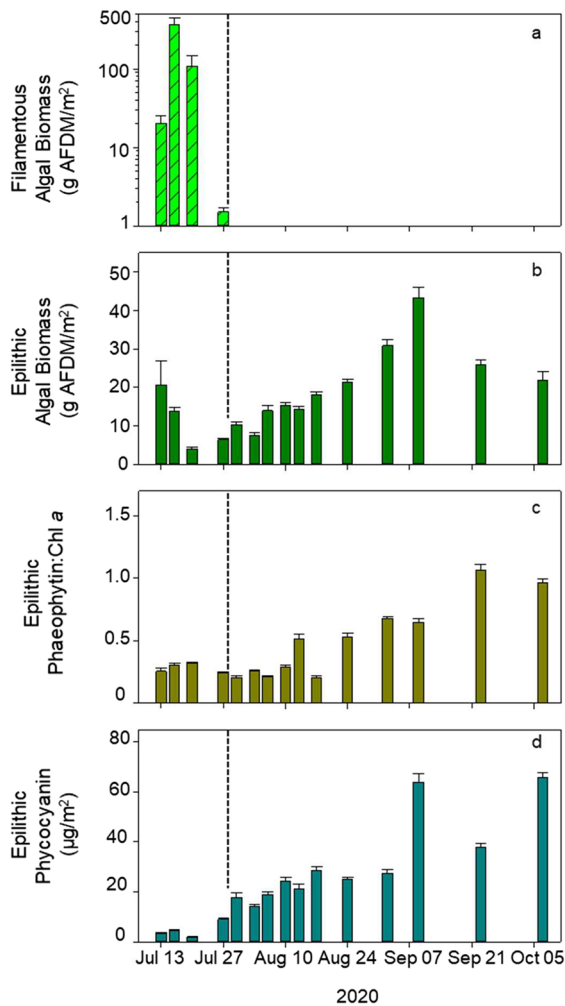

Fig. 6 Concentrations (mg/L) of dissolved nutrients in river water at Site 3 during the summer growing season in 2020 including **a** inorganic nitrogen species as ammonium-N (NH_4-N) and nitrate–N (NO_3-N) and **b** soluble reactive phosphorus (SRP) along with **c** corresponding atomic N:P ratios. Dashed horizontal line in **c** indicates the Redfield N:P ratio of 16. Data are means $\pm$ SE (n = 3 per date)

Fig. 7 Growing season progression of periphyton metrics for incubated benthic primary producers. **a** Filamentous algal biomass (g AFDM/m²), **b** epilithic biomass (g AFDM/m²), **c** epilithon phaeophytin to chl *a* ratios, **d** phycocyanin standing crop (µg/m²). Vertical lines indicate the separation between phases dominated by filamentous and epilithic algae. Bars are mean values plus standard error

vs. time, $R^2 = 0.49$, $p = 0.011$, n = 11) from an average of 6.5 ± 0.3 g AFDM/m² to a peak of 43.3 ± 2.7 g AFDM/m² on September 9th (Fig. 7b), then declined during the final two sampling dates to values 50–60% of maximal standing crop (Fig. 7b). Concurrent with post-filamentous epilithic biomass accumulation, the ratio of phaeophytin to chl *a* (phaeo:chl) in epilithon increased from 0.21 ± 0.01 on August 6th to values closer to a 1 during the last two days of monitoring (Fig. 7c).

Measured phycocyanin standing crops indicated the presence of cyanobacteria throughout periphyton progression. Minimum standing crops of phycocyanin (1.78 ± 0.4 µg/m², July 7th, Fig. 7d) were found during the filamentous phase when *Cladophora* dominated the benthic algal community. Phycocyanin standing crops then increased progressively following the loss of filamentous forms (linear regression of phycocyanin vs. time, $R^2 = 0.75$, $p = 0.0002$, n = 11, Fig. 7d). Towards the end of September, small *Nostoc sp.* nodules were noticeable on rock surfaces. Thereafter, benthic algal community was composed mainly of large grape-sized *Nostoc sp.* nodules and persistent epilithic forms of diatoms and green algae.

Seral assessment of N-fixation rates— physicochemical and biotic drivers: 2020

Rates of N-fixation contrasted sharply between phases of algal progression dominated by filamentous vs. epilithic algae. During the first four monitoring dates, when *Cladophora* was abundant, N-fixation rates were remarkably low (0.007 ± 0.004 mg N/ m²/h, mean $\pm$ SE). On the fifth sampling date, coinciding with the crash in *Cladophora*, N-fixation rates increased to 1.29 ± 0.20 mg N/m²/h (Fig. 8a). The observed increase took place over the course of 3 days (Jul 27th—30th), leading to an average N-fixation rate three orders of magnitude greater than observed during the previous sampling date. Rates of N-fixation remained high with the average rate peaking at 3.29 ± 0.32 mg N/m²/h, and 5.80 mg N/m²/h observed as the maximal rate for single chamber, on August 17th, 18 days after the onset of enhanced rates. Values steadily decreased thereafter, reaching a minimum of 0.07 ± 0.03 mg N/m²/h on September 21st, and increasing to 0.9 ± 0.1 mg N/m²/h on the last day of monitoring (Fig. 8a).

There was little or no evidence that a single environmental variable was closely related to autochthonous N production when employing all data collected for individual dates and chambers (linear regression of N-fixation and environmental variables across chambers and monitoring dates: $p > 0.05$). However, when assessment was restricted to those data collected during the phase dominated by epilithic algae (i.e., after crash of the *Cladophora* bloom), there was very strong evidence for PAR (linear regression of PAR vs. N-fixation rate, $R^2 = 0.48$, $p < 0.0001$,

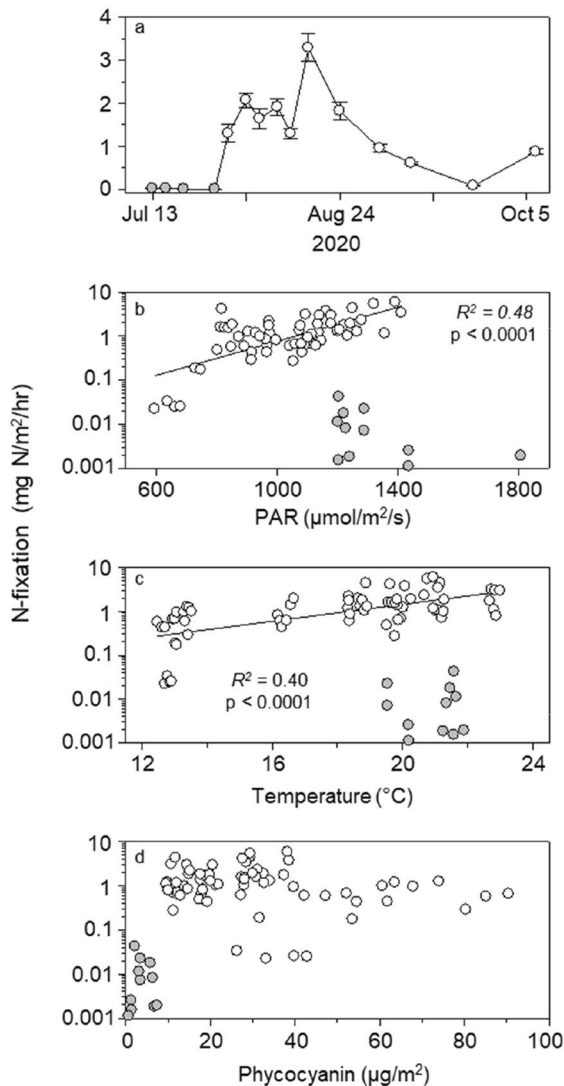**Fig. 8 a** Mean (± standard error) for rates of N-fixation over the course of the growing season at Site 3. Relationships between N-fixation rates and **b** average photon flux density (μmol/m²/s) for photosynthetically active radiation (PAR) during chamber incubation, **c** average water temperature (°C), and **d** phycocyanin standing crop (μg/m²) on the surface of incubated cobbles. Grey symbols indicate assay periods when filamentous algae were notably present on benthic substrate. Solid lines represent significant log-linear regressions derived between variables, excluding data collected during the filamentous phase

Table 2 Results for alternative models generated by stepwise linear regression for evaluating environmental controls over N-fixation rates during the epilithic phase of algal succession

Model	logLik	AIC	ΔAIC	$R^2_{(adj)}$
PAR + temperature + phyco-cyanin	7.84	− 5.68	0	0.63
PAR + temperature	4.01	− 0.02	5.66	0.58
Temperatue + phycocyanin	2.60	2.79	8.47	0.56
PAR	− 2.72	11.44	17.12	0.47
PAR + phyocyanin	− 4.68	15.37	21.05	0.43
Temperature	− 4.37	16.75	22.44	0.42
Phycocyanin	− 18.40	42.81	48.49	0.02
Intercept	− 19.45	42.92	48.60	0

LogLik is the the Log Likelihood of the model, with increasing (less negative) values indicating greater goodness of fit. AIC indicates the Akaike Information Criterion score with smaller values indicating higher relative model quality. ΔAIC indicates the deviation of the Akaike Information Criterion from the best model. A ΔAIC < 2 indicates no statistical differences between models

$R^2_{(adj)}$ indicates the coefficient of determination of the model adjusted for the number of predictors included

alone were related to N-fixation rates regardless of whether analysis included all data or was restricted to the epilithon phase (linear regression of phycocyanin vs. N-fixation rate across days; p > 0.1, Fig. 8d). However, when addressed in combination, temperature, PAR, and phycocyanin together accounted for 63% of the variation in N-fixation rates following the loss of significant *Cladophora* cover (stepwise multiple linear regression of N-fixation rates and environmental measures over 66 observations and eleven sampling dates, Table 2). Finally, there was weak evidence linking ambient DIN to N-fixation rates (linear regression of DIN concentration and N-fixation rate across 14 days: $R^2 = 0.23$, $p = 0.09$, n = 13; Fig. S4a in Supplemental Information) while extremely strong evidence suggested that SRP concentrations declined exponentially with increasing N-fixation (non-linear regression of SRP and N-fixation rates across 14 days: $R^2 = 0.74$, $p < 0.0001$, n = 13, Fig. S4b in Supplemental Information).

Discussion

This study presents evidence that algal communities in the UCFR respond to snowmelt with enhanced

Fig. 8b) and temperature (linear regression of water temperature vs. N-fixation rate, $R^2 = 0.43$ $p < 0.0001$, Fig. 8c) stimulation of N-fixation. Despite its specific association with cyanobacteria, there was little or no evidence that phycocyanin standing crops

primary production (Prater 2021), biomass accrual, and compositional succession characteristic of systems where annual spring floods are the main source of hydrologic disturbance (Poff and Ward 1989; Yarnell et al. 2010). This identifies the UCFR, and other snowmelt-dominated systems, as belonging to a class of running waters organized by successional processes as previously observed for prairie streams (Tate 1990), desert streams (Fisher et al. 1982), and other open-channel mid-sized rivers experiencing hydrologic disturbance (Uehlinger and Naegeli 1998a, b; Power et al. 2008; Gillett et al. 2016).

In the UCFR, snowmelt dominates the disturbance regime and initiates recession responses with early season establishment and accumulation of the filamentous green algae *C. glomerata*. (Dodds et al. 1997; Suplee et al. 2012). Here we emphasize successional progression to include late seasonal assemblages more dominated by cyanobacteria during warm conditions of depleted reactive N concentrations. Whether following an abrupt die-off of *Cladophora* over a number of days, or in concert with prolonged declines in abundance of filamentous green algae, all of our study sites shifted towards increased epilithic cyanobacteria during later stages of the growing season. While the recurrent blooms of *Cladophora* in the UCFR are known to river scientists (Dodds et al. 1997; Flynn and Chapra 2014; Valett et al. 2022) and water resource managers (Suplee et al. 2009), our investigation is the first to record the successional progression toward cyanobacterial dominance of the periphyton, with implications for ecosystem function and water quality management.

Succession and the biogeochemical template – abiotic and biotic drivers

Annual changes in the biogeochemical template of the UCFR are driven by linkages to the surrounding landscape and the progression of in-stream biota. Contrasting temporal patterns for N and P suggest alternative flowpaths, with seasonally connected sources important during high flow and others dominant during baseflow as seen in other systems (Mulholland and Hill 1997). Highest concentrations of DIN during the dormant season and steep declines during snowmelt suggest that N-rich allochthonous sources influential during the winter were diluted during runoff as seen historically in the UCFR (Valett

et al. 2022) and in a myriad of other lotic systems world-wide (Goodale et al. 2009 and references therein). In contrast, maximum SRP concentrations observed during periods of greatest flow suggest rich sources of P linked to the river when water tables are elevated. For the UCFR, natural sedimentary deposits of P (Carey 1991; Ingman 1992) and enhanced delivery related to their extraction (Knudsen et al. 2002) likely lead to waters replete in P, even during low-flow conditions. While both DIN and SRP concentrations were minimal at low flow, SRP concentrations appear to remain above limiting levels as suggested by atomic N:P ratios remaining less than the Redfield ratio throughout the growing season.

Flooding and historical RABs

Annual RABs dominated by *Cladophora* remain characteristic of the UCFR. Our analysis shows that over the 21 years of monitoring, RABs dominated by *Cladophora* have not declined and remain in excess of the 100 mg/m^2 water quality standard established by the Montana Department of Environmental Quality (Dodds et al. 1997; Suplee et al. 2007, 2009). Our results extend the temporal range of observations by Suplee et al. (2012) and are in agreement with the conclusion that earlier efforts at nutrient reduction (Tri State Water Council 2009), and those currently in place, have failed to notably alter the frequency or magnitude of RABs in the UCFR.

The intensity of RAB development in the UCFR is, in part, regulated by the river's disturbance regime. We found a negative correlation between the intensity of snowmelt disturbance (i.e., peak discharge) and average growing season periphyton abundance, indicating that floods of greater magnitude may delay biomass accrual. In contrast, the magnitude of flows in previous years does not seem to influence the size of the bloom during any given growing season. Eilers et al. (2022) showed that high spring flows in the Deschutes River, Oregon, USA, were responsible for lower standing crops of *Cladophora* due to scouring of basal holdfasts requiring recolonization and delaying accrual. Flooding in upstream reaches of the UCFR is moderated by holding ponds erected at the river's origin (Fig. 1), designed to promote settling of particulate mine contaminants (Phillips and Lipton 1995), which may influence how hydrologic

disturbance modulates RAB development along the river's length.

Cladophora accrual and decline during snowmelt recession

Maximal algal standing crops dominated by *Cladophora* were observed immediately after the beginning of flow recession and were generally followed by steep decline following peak snowmelt. Recent work has emphasized the propensity for the development of extensive mats to promote self-shading in *Cladophora* (Higgins et al. 2008; Flynn et al. 2018) resulting in cells near the base of the mats becoming increasingly susceptible to detachment and sloughing. Banish (2017) documented extensive *Cladophora* sloughing and drift in the UCFR that lagged maximal benthic biomass by ca. two weeks.

In other systems displaying comparable RAB succession, complex food web dynamics have the potential to modulate the growth and productivity of algae. Progression of *Cladophora* blooms in the Eel River, CA, includes the establishment of epiphytic diatoms that display distinct phases of density and composition leading to proliferation of N-fixing genus *Epithemia* (Power et al. 2009; Furey et al. 2012). Midge grazing and retreat construction alters epiphytic abundance and may promote *Cladophora* health (Furey et al. 2012). In the UCFR, we observed phases of epiphyte colonization prior to senescence comparable to those described by Power et al. (2009), but the community was dominated by the genus *Cocconeis* (H.M. Valett, unpublished data), recognized as opportunistic colonizers of highly disturbed environments (Biggs et al. 1998), and as a common non-fixing epiphyte found on *Cladophora* (Furey et al. 2012). While no direct work has assessed their role in the UCFR, we observed no evidence of tuft building midges or large-bodied grazers capable of controlling *Cladophora* mat development. In the apparent absence of effective removal by grazers, shading by epiphytic colonists may further facilitate the senescence of *Cladophora* and subsequent shifts in RAB composition over time.

Nutrient dynamics and N-fixation along the successional gradient

Changes in autotrophic form and abundance in the UCFR coincided with changes in ecosystem N and P cycling. Following an extended periods of water column N:P ratios well below the Redfield ratio of 16, rates of N-fixation increased abruptly with successional change in algal cover. During the early filamentous phase, *Cladophora* appeared to suppress cyanobacterial abundance and activity, potentially favoring non-fixing forms, or suppressing N-fixation directly via local shading. Later, the benthic community dominated by cyanobacteria nodules supported N-fixation rates among the highest reported for lotic systems (Grimm and Petrone 1997; Kunza and Hall 2014). Thus, distinct change in autotrophic cover appears linked to a functional shift towards N-fixation, a process tied quantitatively to PAR, temperature, and phycocyanin standing crop.

Contrary to other studies that found N fixation to be controlled by DIN availability (Grimm and Petrone 1997; Kunza and Hall 2013), we found that N-fixation demonstrated a weak positive relationship with local N availability with NH_4-N as the dominant available form. The origin of the NH_4-N and reasons for its persistence in the water column are unknown, but concentrations in this range have been observed elsewhere in the UCFR (Banish 2017; Valett et al. 2022). The range of DIN concentrations observed in our study (0.003–0.022 mg/L) was rather constrained when compared to others (e.g., 0.004–0.050 mg/L, Grimm and Petrone 1997; 0–>0.300 mg/L, Kunza and Hall 2014), but recent work suggests a more complicated relationship between DIN availability and rates of N-fixation.

Eberhard et al. (2018) noted that across systems within a semi-arid mountainous catchment where DIN concentrations ranged from 26–615 μg/L, streams with greatest DIN concentrations did not display lowest N-fixation rates. In fact, the stream with the second greatest DIN concentration (506 μg/L) displayed the highest rate of sediment N-fixation. Further, when combined with other chemical variables in a multiple regression approach, no significant model was found to predict N-fixation. In response, Eberhard et al. proposed that factors occurring at smaller scales may influence autochthonous N production, a perspective echoed by Marcarelli et al. (2022) who emphasized diazotroph diversity, its influence on rate variability, and the challenges of scale when addressing controls over aquatic N-fixation.

We also found a negative correlation between SRP concentrations in the water column and N-fixation

rates. Others have emphasized the potential for N-fixation to deplete P availability and regulate rates in the open ocean (Karl et al. 1997; Wu et al. 2000). On the other hand, P enrichment in streams has been found to increase the abundance of N-fixing taxa (e.g., Elwood et al. 1981) and N-fixation rates (Marcarelli and Wurtsbaugh 2006). These combined responses suggest that cyanobacterial primary productivity and N-fixation may exert strong controls over water NH_4-N and SRP concentrations during the later stages of the growing season within a given system, while environmental pools may dictate rates over larger spatial and temporal scales (Finlay et al. 2011; Eberhard et al. 2018).

Ecosystem implications of N-fixation for the UCFR

Autochthonous N production during the late stages of the growing season may subsidize primary production and maintain late successional autotrophic activity in the UCFR. During later epilithic phases, *Nostoc* was the main primary producer and the system achieved peak epilithic standing crops at times of lowest N:P ratio. Based on the net biomass increment calculated from the linear growth phase for epilithon, rates of accumulation were ca. 162 mg C/m^2/d, while net primary production was likely much higher given sloughing and grazing as alternative fates for periphyton biomass. Using the canonical C:N ratio for algae (6.625, Redfield 1958) or a higher value observed for cyanobacteria in a eutrophic lake (9.5, Leonardson 1984), biomass accumulation during the epilithic phase translates to an N-demand between 19.9 and 28.5 mg N/m^2/d. When conservatively applied to an 8-h photoperiod, rates of N-fixation observed during our field assays ranged from a maximum of 26.3 mg N/m^2/d to an average of 10.5 mg N/m^2/d. These calculations suggest that N-fixation has the potential to supply from 37 to 132% of concomitant periphyton N demand. Thus, N-fixation rates appear to be of sufficient magnitude to maintain autotrophic growth during times of apparent N-limitation.

The implications of autochthonous N-fixation are further understood when compared to other sources of N potentially fueling biotic demand. Kunza and Hall (2014) showed that N-fixation accounted for up to 8 times the total uptake of inorganic N in low-nutrient streams rich in cyanobacteria and N-fixing diatoms species. Using a budgetary approach, Grimm

and Petrone (1997) represented N-fixation as a percentage of combined inputs (i.e., N retention via assimilation of DIN plus N-fixation) and showed that autochthonous N acquisition could supply from less than 20 to as much as 85% of N demand in Sycamore Creek, AZ, USA. We did not measure net N uptake, but using growing season mass-balance values generated for a similar stretch of the UCFR (10–60 mg N/m^2/d; Valett et al. 2022), N-fixation rates from our study would average between 30 and 50% of total uptake. These values suggest that nearly comparable reliance on existing bioavailable DIN and autochthonous N production may be characteristic of the N economy during late stages of succession.

Conclusions

Results presented here document the well-known occurrence of RABs in the UCFR, but extend that observation to include temporal progression of algal communities during snowmelt recession. Blooms progress from abundant green algae in N-rich waters soon after snowmelt to secondary blooms of cyanobacteria during later stages of the growing season when warm waters are N-poor. RABs form following snowmelt scour and historical data show that bloom magnitude is in part regulated by disturbance intensity.

Our work emphasizes the successional progression of the river's biogeochemical template from one initially driven by exogenous influences to later stages driven by endogenous biotic processes, as seen temporally in other systems (Fisher et al. 1982; Valett et al. 2008). Along with studies addressing the time course of biogeochemical behavior in the UCFR for materials like organic carbon (Young 2022) and inorganic N (Valett et al. 2022), our findings suggest early influence of external sources, with materials supplied through tributary or groundwater inputs, followed by a transition to endogenous N retention and autochthonous N-fixation. Thus, progression includes enrichment through hydrologic connection followed by enhanced productivity and autochthony during recession, a model congruent with that proposed by Yarnell et al. (2010) to govern succession during snowmelt recession.

There has been a long history of work arguing for the importance of autotrophy in lotic systems

(Minshall 1978; Busch and Fisher 1981; Thorp and Delong 1994; Uehlinger and Naegeli 1998a, b) and it has progressed toward a more general understanding of the role of autochthony in stream food webs (Finlay 2001; Thorp and Delong 2002), including consideration of limiting nutrients and the importance of autochthonous N-fixation (Marcarelli et al. 2008; Welter et al. 2015). In the UCFR, the proliferation of autochthonous N production during late phases of the growing season was related to warming temperatures during periods of low DIN concentrations. Welter et al. (2015) emphasized the temperature dependence of N-fixation as indicated by the apparent activation energies reported across a broad range of stream temperatures. Moreover, their work indicated enhanced temperature dependence of ecosystem metabolism (gross primary production and respiration) resulting from the stimulatory role of N-fixation. Thus, late successional autochthonous N production may sustain the considerable rates of autotrophic production characteristic of the UCFR (Prater 2021; Trentman et al. 2023). These results suggest that successional development of autochthony in rivers like the UCFR involves multiple elements, promotes interaction between the carbon and N cycles, and emphasizes the important role for resource supply when considering ecosystem responses to warming (Yvon-Durocher et al. 2012; Welter et al. 2015).

Declarations

References

Banish NJ (2017) Factors influencing Cladophora biomass abundance in the Upper Clark Fork River. University of Montana, Montana

Bartoń K (2017) MuMIn: Multi-model Inference. Version 1.40.0

Bennett MG, Schofield KA, Lee SS, Norton SB (2017) Response of chlorophyll a to total nitrogen and total phosphorus concentrations in lotic ecosystems: a systematic review protocol. Environ Evid 6:18. https://doi.org/10.1186/s13750-017-0097-8

Biggs B, Stevenson RJ, Lowe RL (1998) A habitat matrix conceptual model for stream periphyton. Arch Fur Hydrobiol 143:21–56. https://doi.org/10.1127/archiv-hydrobiol/143/1998/21

Biggs BJF (1996) Hydraulic habitat of plants in streams. Regul Rivers Res Manag 12:131–144

Biggs BJF (2000) Eutrophication of streams and rivers: dissolved nutrient-chlorophyll relationships for benthic algae. J North Am Benthol Soc 19:17–31. https://doi.org/10.2307/1468279

Bothwell ML, May N (1985) Phosphorus limitation of lotic periphyton growth rates. Water Res 30:527–542

Bruns NE, Heffernan JB, Ross MRV, Doyle M (2022) A simple metric for predicting the timing of river phytoplankton blooms. Ecosphere 13:e4348. https://doi.org/10.1002/ecs2.4348

Burnham KP, Anderson DR (2002) Model selection and multimodel inference: a practical information-theoretic approach, 2nd edn

Busch DE, Fisher SG (1981) Metabolism of a desert stream. Freshw Biol 11:301–308

Capone DG (2018) Determination of nitrogenase activity in aquatic samples using the acetylene reduction procedure. In: Kemp PF, Cole JJ, Sherr BF, Sherr EB (eds) Handbook of methods in aquatic microbial ecology. CRC Press, Boca Raton, pp 621–631

Carey JH (1991) Phosphorus sources in Gold Creek a tributary of the Clark Fork River in western Montana

Council TSWQ, Council TSWQ (2009) The Clark Fork River Voluntary Nutrient Reduction Program 1998–2008. The progress of a voluntary program in reducing nutrients and noxious algae in the Clark Fork River in Montana. Tri State Water Quality Council, Sandpoint, ID

Cremella B, Huot Y, Bonilla S (2018) Interpretation of total phytoplankton and cyanobacteria fluorescence from cross-calibrated fluorometers, including sensitivity to turbidity and colored dissolved organic matter. Limnol Oceanogr Methods 16:881–894. https://doi.org/10.1002/lom3.10290

D'Andrilli J, Peipoch M, Payn RA et al (2021) Collaborative achievements and challenges for our 10-YR river research effort. Limnol Oceanogr Bull 30:127–128. https://doi.org/10.1002/lob.10465

Davis CJ, Fritsen CH, Wirthlin ED, Memmott JC (2012) High rates of primary productivity in a semi-arid tailwater: implications for self-regulated production. River Res Appl 28:1820–1829. https://doi.org/10.1002/rra.1573

Dodds WK, Gudder DA (1992) The ecology of Cladophora. J Phycol 28:415–427. https://doi.org/10.1111/j.0022-3646.1992.00415.x

Dodds WK, Lopez AJ, Bowden WB et al (2002) N uptake as a function of concentration in streams. JNABS 21:206–220

Dodds WK, Smith VH (2016) Nitrogen, phosphorus, and eutrophication in streams. Inl Waters 6:155–164. https://doi.org/10.5268/IW-6.2.909

Dodds WK, Smith VH, Zander B (1997) Developing nutrient targets to control benthic chlorophyll levels in streams: a case study of the Clark Fork River. Water Res 31:1738–1750. https://doi.org/10.1016/s0043-1354(96)00389-2

Eberhard EK, Marcarelli AM, Baxter CV (2018) Co-occurrence of in-stream nitrogen fixation and denitrification across a nitrogen gradient in a western U.S. watershed. Biogeochemistry 139:179–195. https://doi.org/10.1007/s10533-018-0461-y

Eilers JM, Davis CJ, Vander Meer D, Vache K (2022) Spring peak flows control abundance of Cladophora in a Hydropower-Impacted River. River Res Appl. https://doi.org/10.1002/rra.4041

Elwood JW, Newbold JD, Trimble AF, Stark RW (1981) The limiting role of phosphorus in a Woodland stream ecosystem: effects of P enrichment on leaf decomposition and primary producers. Ecology 62:146–158. https://doi.org/10.2307/1936678

EPA (1993a) Method 353.2, Revision 2.0: determination of nitrate-nitrite nitrogen by automated colorimetry 1–14

EPA (1993b) Method 350.1, Revision 2.0: determination of ammonia nitrogen by semi-automated colorimetry 1–14

EPA (1993c) Method 365.1, Revision 2.0: determination of phosphorus by semi-automated colorimetry. Environ Monit Syst Lab 1–15

Finlay JC (2001) Stable-carbon-isotope ratios of river biota:implications for energy flow in lotic food webs. Ecology 82:1052–1064. https://doi.org/10.1890/0012-9658(2001)082[1052:SCIROR]2.0.CO;2

Finlay JC, Hood JM, Limm MP et al (2011) Light-mediated thresholds in stream-water nutrient composition in a river network. Ecology 92:140–150. https://doi.org/10.1890/09-2243.1

Fisher SG, Gray LJ, Grimm NB, Busch DE (1982) Temporal succession in a desert stream ecosystem following flash flooding. Ecol Monogr 52:93–110. https://doi.org/10.2307/2937346

Flynn KF, Chapra SC (2014) Remote sensing of submerged aquatic vegetation in a shallow non-turbid river using an unmanned aerial vehicle. Remote Sens 6:12815–12836. https://doi.org/10.3390/rs61212815

Flynn KF, Chudyk W, Watson V et al (2018) Influence of biomass and water velocity on light attenuation of Cladophora glomerata L. (Kuetzing) in rivers. Aquat Bot 151:62–70. https://doi.org/10.1016/j.aquabot.2018.08.002

Furey PC, Lowe RL, Power ME, Campbell-Craven AM (2012) Midges, Cladophora, and epiphytes: shifting interactions through succession. Freshw Sci 31:93–107. https://doi.org/10.1899/11-021.1

Gardner JR, Ensign SH, Houser JN, Doyle MW (2020) Light exposure along particle flowpaths in large rivers. Limnol Oceanogr 65:128–142. https://doi.org/10.1002/lno.11256

Gillett ND, Pan Y, Eli Asarian J, Kann J (2016) Spatial and temporal variability of river periphyton below a hypereutrophic lake and a series of dams. Sci Total Environ 541:1382–1392. https://doi.org/10.1016/j.scitotenv.2015.10.048

Goodale CL, Thomas SA, Fredriksen G et al (2009) Unusual seasonal patterns and inferred processes of nitrogen retention in forested headwaters of the Upper Susquehanna River. Biogeochemistry 93:197–218. https://doi.org/10.1007/s10533-009-9298-8

Grimm NB (1987) Nitrogen dynamics during succession in a desert stream. Ecology 68:1157–1170

Grimm NB, Petrone KC (1997) Nitrogen fixation in a desert stream ecosystem. Biogeochemistry 37:33–61

Hallegraeff GM (2003) Harmful algal blooms: a global overview. Man Harmful Mar Microalgae 33:1–22

Heffernan JB, Liebowitz DM, Frazer TK et al (2010) Algal blooms and the nitrogen-enrichment hypothesis in Florida springs: evidence, alternatives, and adaptive management. Ecol Appl 20:816–829. https://doi.org/10.1890/08-1362.1

Heisler J, Glibert PM, Burkholder JM et al (2008) Eutrophication and harmful algal blooms: a scientific consensus. Harmful Algae 8:3–13. https://doi.org/10.1016/j.hal.2008.08.006

Higgins SN, Hecky RE, Guildford SJ (2008) The collapse of benthic macroalgal blooms in response to self-shading. Freshw Biol 53:2557–2572. https://doi.org/10.1111/j.1365-2427.2008.02084.x

Ingman GL (1992) Assessment of phosphorus and nitrogen sources in the Clark Fork River Basin, 1988–1991, Final Report, Section 525 of te 1987 Clean Water Act Amendments. Montana Department of Health and Environmental Services, Division of Water Quality, Helena, MT

Karl D, Letelier R, Tupas L et al (1997) The role of nitrogen fixation in biogeochemical cycling in the subtropical North Pacific Ocean. Nature 388:533–538. https://doi.org/10.1038/41474

Knudsen AC, Gunter ME, Herring JR et al (2002) Mineralogical characterization of weathered and less weathered strata of the Meade Peak phosphatic shale member of the Permian Phosphoria Formation; measured sections E and

F, Rasmussen Ridge, and measured sections G and H, Sage Creek area of the Webster

Kunza LA, Hall RO (2013) Demographic and mutualistic responses of stream nitrogen fixers to nutrients. Freshw Sci 32:991–1004. https://doi.org/10.1899/12-102.1

Kunza LA, Hall RO (2014) Nitrogen fixation can exceed inorganic nitrogen uptake fluxes in oligotrophic streams. Biogeochemistry 121:537–549. https://doi.org/10.1007/s10533-014-0021-z

Kyro C (2021) Nitrogen dynamics and transport along flowpaths in a rural wetland-stream complex Let us know how access to this document benefits you

Lake PS (2008) Flow-generated disturbances and ecological responses: floods and droughts. In: Wood DMH, Sadller JP (eds) Hydroecology and ecohydrology: past, present, and future. Willey Press, New York, pp 75–92

Leonardson L (1984) Does N2 fixation meet the nitrogen requirements of heterocystous blue-green algae in shallow eutrophic lakes? Oecologia 63:398–404. https://doi.org/10.1007/BF00390672

Marcarelli AM, Baker MA, Wurtsbaugh WA (2008) Is in-stream N_2 fixation an important N source for benthic communities and stream ecosystems? J North Am Benthol Soc 27:186–211. https://doi.org/10.1899/07-027.1

Marcarelli AM, Fulweiler RW, Scott JT (2022) Nitrogen fixation: a poorly understood process along the freshwater-marine continuum. Limnol Oceanogr Lett 7:1–10. https://doi.org/10.1002/lol2.10220

Marcarelli AM, Wurtsbaugh WA (2006) Temperature and nutrient supply interact to control nitrogen fixation in oligotrophic streams: an experimental examination. Limnol Ocean 51:2278–2289. https://doi.org/10.4319/lo.2006.51.5.2278

Marcarelli AM, Wurtsbaugh WA (2009) Nitrogen fixation varies spatially and seasonally in linked stream-lake ecosystems. Biogeochemistry 94:95–110. https://doi.org/10.1007/s10533-009-9311-2

Marcarelli AM, Wurtsbaugh WA (2014) Fixation varies spatially and seasonally in linked stream-lake ecosystems. Biogeochemistry 94:95–110. https://doi.org/10.1007/s10533-009-931

McAllister TG, Wood SA, Hawes I (2016) The rise of toxic benthic Phormidium proliferations: a review of their taxonomy, distribution, toxin content and factors regulating prevalence and increased severity. Harmful Algae 55:282–294. https://doi.org/10.1016/j.hal.2016.04.002

Menard S (2001) Logistic regression analysis, 2nd edn. Sage Publications, Thousand Oaks

Minshall GW (1978) Autotrophy in stream ecosystems. Bioscience 28:767–771. https://doi.org/10.2307/1307250

Moore JN, Langer HW (2012) Can a river heal itself? Natural attenuation of metal contamination in river sediment. Environ Sci Technol 46:2616–2623. https://doi.org/10.1021/es203810j

Moss B (2012) Cogs in the endless machine: lakes, climate change and nutrient cycles: a review. Sci Total Environ 434:130–142. https://doi.org/10.1016/j.scitotenv.2011.07.069

Moulton T, Souza M, Walter T et al (2009) Patterns of periphyton chlorophyll and dry mass in a neotropical stream: a cheap and rapid analysis using a hand-held fluorometer. Mar Freshw 60:224–233

Mulholland PJ, Hill WR (1997) Seasonal patterns in streamwater nutrient and dissolved organic carbon concentrations: Separating catchment flow path and in-stream effects. Water Resour Res 33:1297–1306. https://doi.org/10.1029/97WR00490

Paerl HW, Fulton RS, Moisander PH, Dyble J (2001) Harmful freshwater algal blooms, with an emphasis on cyanobacteria. Sci World J 1:76–113. https://doi.org/10.1100/tsw.2001.16

Paerl HW, Otten TG, Kudela R (2018) Mitigating the expansion of harmful algal blooms across the freshwater-to-marine continuum. Environ Sci Technol 52:5519–5529. https://doi.org/10.1021/acs.est.7b05950

Peterson CG, Valett HM, Dahm CN (2001) Shifts in habitat template for lotic microalgae linked to interannual variation in snowmelt intensity. Limnol Oceanogr 46:858–870

Phillips G, Lipton J (1995) Injury to aquatic resources caused by metals in Montana's Clark Fork River basin: historic perspective and overview. Can J Fish Aquat Sci 52:1990–1993

Poff NL (1992) Why disturbances can be predictable: a perspective on the definition of disturbance in streams. J North Am Benthol Soc 11:86–92. https://doi.org/10.2307/1467885

Poff NL, Ward JV (1989) Implications of streamflow variability and predictability for lotic community structure: a regional analysis of streamflow patterns. Can J Fish Aquat Sci 46:1805–1818

Power M, Lowe R, Furey P et al (2009) Algal mats and insect emergence in rivers under Mediterranean climates: towards photogrammetric surveillance. Freshw Biol 54:2101–2115. https://doi.org/10.1111/j.1365-2427.2008.02163.x

Power ME, Parker MS, Dietrich WE (2008) Seasonal reassembly of a river food web: floods, droughts, and impacts of fish. Ecol Monogr 78:263–282

Prater JA (2021) Controls on NO3-N dynamics in the Upper Clark Fork River, Montana. MS thesis, University of Montana

Redfield AC (1958) The biological control of chemical factors in the environment. Am Sci Autumn 46:205–221

Sabater S, Vilalta E, Gaudes A et al (2003) Ecological implications of mass growth of benthic cyanobacteria in rivers. Aquat Microb Ecol 32:175–184. https://doi.org/10.3354/ame032175

Smith VH (1983) Low nitrogen to phosphorus ratios favor dominance by blue-green algae in lake phytoplankton. Science 221:669–671. https://doi.org/10.1126/science.221.4611.669

Steinman A, Lamberti G, Leavitt P, Uzarski D (2017) Biomass and pigments of benthic algae. In: Methods in stream ecology, 3rd edn, pp 223–241

Suplee MW, Varghese A, Cleland J (2007) Developing nutrient criteria for streams: an evaluation of the frequency distribution method1. JAWRA J Am Water Resour Assoc 43:453–472. https://doi.org/10.1111/j.1752-1688.2007.00036.x

Suplee MW, Watson V, Teply M, McKee H (2009) How green is too green? Public opinion of what constitutes undesirable algae levels in streams. J Am Water Resour Assoc 45:123–140. https://doi.org/10.1111/j.1752-1688.2008.00265.x

Suplee MW, Watson V, Dodds WK, Shirley C (2012) Response of algal biomass to large-scale nutrient controls in the Clark Fork River, Montana, United States. JAWRA 48:1008–1021. https://doi.org/10.1111/j.1752-1688.2012.00666.x

Tate CM (1990) Patterns and controls of nitrogen in tallgrass prairie streams. Ecology 71:2007–2018

Thorp JH, Delong MD (1994) The Riverine productivity model: an heuristic view of carbon sources and organic processing in large river ecosystems. Oikos 70:305–308. https://doi.org/10.2307/3545642

Thorp JH, Delong MD (2002) Dominance of autochthonous autotrophic carbon in food webs of heterotrophic rivers. Oikos 96:543–550. https://doi.org/10.1034/j.1600-0706.2002.960315.x

Trentman M, Hall RO, Valett HM (2023) Exploring the mismatch between theory and application of the photosynthetic quotient in aquatic ecosystems. Limnol Lett. https://doi.org/10.1002/lol2.10326

Uehlinger U, Naegeli MW (1998a) Ecosystem metabolism, distrubance, and stability in a prealpine gravel bed river. J North Am Benthol Soc 17(2):165–178

Uehlinger U, Naegeli MW (1998b) Ecosystem metabolism, disturbance, and stability in a prealpine gravel bed river. J North Am Benthol Soc 17:165–178. https://doi.org/10.2307/1467960

Vadeboncoeur Y, Power ME (2017) Attached algae: the cryptic base of inverted trophic pyramids in freshwaters. Annu Rev Ecol Evol Syst 48:255–279. https://doi.org/10.1146/annurev-ecolsys-121415-032340

Valett HM, Peipoch M, Poole GC (2022) Nutrient processing domains: spatial and temporal patterns of material retention in running waters. Freshw Sci 41:195–214. https://doi.org/10.1086/719991

Valett HM, Thomas SA, Mulholland PJ et al (2008) Endogenous and exogenous control of ecosystem function: N cycling in headwater streams. Ecology 89:3515–3527. https://doi.org/10.1890/07-1003.1

Welter JR, Benstead JP, Cross WF et al (2015) Does N_2 fixation amplify the temperature dependence of ecosystem metabolism? Ecology 96:603–610. https://doi.org/10.1890/14-1667.1

Wood SA, Kelly LT, Bouma-Gregson K et al (2020) Toxic benthic freshwater cyanobacterial proliferations: challenges and solutions for enhancing knowledge and improving monitoring and mitigation. Freshw Biol 65:1824–1842. https://doi.org/10.1111/fwb.13532

Wu J, Sunda W, Boyle EA, Karl DM (2000) Phosphate depletion in the Western North Atlantic Ocean. Science 289:759–762. https://doi.org/10.1126/science.289.5480.759

Yarnell SM, Viers JH, Mount JF (2010) Ecology and management of the spring snowmelt recession. Bioscience 60:114–127. https://doi.org/10.1525/bio.2010.60.2.6

Young FL (2022) Characterizing riverine carbon: a spatiotemporal study of organic and inorganic carbon variability and evaluation of methods for quantifying pCO2. PhD dissertation, University of Montana

Yvon-Durocher G, Caffrey JM, Cescatti A et al (2012) Reconciling the temperature dependence of respiration across timescales and ecosystem types. Nature 487:472–476. https://doi.org/10.1038/nature11205

Publisher's Note   Springer Nature remains neutral with regard to jurisdictional claims in published maps and institutional affiliations.